Snowpack radiative heating: Influence on Tibetan Plateau climate

Mark G. Flanner and Charles S. Zender

Department of Earth System Science, University of California, Irvine, California, USA

Received 23 November 2004; revised 19 January 2005; accepted 15 February 2005; published 16 March 2005.

[1] Solar absorption decays exponentially with depth in snowpacks. However, most climate models constrain all snowpack absorption to occur uniformly in the top-most snow layer. We show that 20–45% of solar absorption by deep snowpacks occurs more than 2 cm beneath the surface. Accounting for vertically-resolved solar heating alters steady-state snow mass without changing bulk snow albedo, and ice-albedo feedback amplifies this effect. Vertically-resolved snowpack heating reduces winter snow mass on the Tibetan Plateau by 80% in one GCM, and significantly increases 2 m air temperature. These changes significantly reduce model-measurement discrepancies. Our results demonstrate that snowpack radiative heating plays a significant role in regulating surface climate and hydrology. More accurate snowpack radiation has the potential to improve predictions of related climate processes, such as spring runoff and the Asian Monsoon. **Citation:** Flanner, M. G., and C. S. Zender (2005), Snowpack radiative heating: Influence on Tibetan Plateau climate, *Geophys. Res. Lett.*, *32*, L06501, doi:10.1029/2004GL022076.

1. Introduction

[2] Net surface solar radiation often dominates the energy budget of snow melt processes in non-forested areas and hence influences snow thickness, extent, and surface albedo in many regions [*Molotch et al.*, 2004]. Winter mean snowpack absorption can reach 50 W m^{-2} or more, depending on local insolation and snow age. Sophisticated snow and ice radiation models predict realistic vertical distributions of solar absorption [e.g., *Grenfell*, 1991; *Jordan*, 1991]. However, general circulation models (GCMs) typically deposit all absorbed solar radiation in the top-most snow layer. Unrealistic representation of snow-radiation interactions may bias climate predictions in snowy regions, especially mid-latitude regions where insolation is relatively intense. *Foster et al.* [1996] analyzed seven GCMs and found a nearly ubiquitous over-prediction of snow depth in the Tibetan Plateau (TP) region (30–40°N, 80–100°E). This paper identifies and assesses climatic implications of vertically-distributed snowpack heating in the TP region.

[3] Accurate representation of snow physical processes on the TP are important for several reasons. The Blanford Hypothesis [*Blanford*, 1884] predicts that springtime TP snow quantity influences the South Asian Monsoon strength. *Fasullo* [2004] shows that in non-ENSO, strong-monsoon years there is a significant negative correlation between snow cover fraction over Tibet and the Himalayas during December–February (DJF) and Indian rainfall in the following June–September. Tibetan winter snow cover is also linked to summer rainfall over the Yangtze River Valley [*Wu and Qian*, 2003]. Late spring snow cover constrains dust emissions from East Asia [*Kurosaki and Mikami*, 2004]. Finally, snow melt and glacial melt-water on the TP help feed ten of Asia's largest rivers, which bring freshwater to about one-half of Earth's population.

0094-8276/05/2004GL022076$05.00

2. Methods

[4] Snowpack heating and reflectance are predicted with our two-stream, multi-layer SNow, ICe, and Aerosol Radiation model (SNICAR), based on *Wiscombe and Warren* [1980] and *Toon et al.* [1989]. The present study neglects aerosol effects. Snow is treated as a collection of ice spheres, lognormally distributed in size, with number median radii $50 \leq r_n \leq 1000$ μm and geometric standard deviation of 2.0. Mie parameters are computed off-line for one visible (0.3–0.7 μm) and four near-infrared (NIR) (0.7–1.0, 1.0–1.2, 1.2–1.5, and 1.5–5.0 μm) spectral bands. This coarse spectral discretization yields vertical flux profiles within 10% of a 10 nm spectral grid. The NIR bands are combined into the single NIR band predicted by the host GCM weighted by a surface insolation distribution appropriate for mid-latitude winter, assuming 30% cloud coverage. *In situ* data on vertical profiles of radiative flux divergence in snowpacks are scarce [*Warren*, 1982]. However, net downward flux from SNICAR is within ~15% of measurements throughout the top meter of one snowpack [*Schwerdtfeger and Weller*, 1977].

[5] SNICAR is implemented in the Community Land Model (CLM) Version 3 [*Oleson et al.*, 2004], the land component of the NCAR Community Atmosphere Model (CAM) Version 3 [*Collins et al.*, 2004]. The snow physics represented in up to five layers include thermal diffusion, density increases from snow compaction, water flow, and vertically resolved melting and re-freezing. SNICAR replaces the original CLM snowpack radiative formulation, which bases snow albedo on an empirical function and constrains solar snowpack absorption to occur in the top 2 cm surface layer.

[6] Table 1 summarizes the two sets of experiments performed. The off-line experiments force CLM with 1990–1999 atmospheric data from the National Center for Environmental Prediction (NCEP) reanalysis project [*Kalnay et al.*, 1996]. These experiments are named CLM-X for model configuration "X". In this uncoupled mode, precipitation and temperature from the lowest atmospheric level are fixed, which tightly constrains land surface climate. Coupled experiments (named CAM-X) use CLM coupled to the CAM3 atmosphere model forced with climate-mean sea surface temperatures. The A experiments use the original CLM snow radiation physics (prescribed albedo, all absorption occurs in top snow layer). The B

Table 1. Numerical Experiments

Off-Line Simulation	Coupled Simulation	Snow RT Model	Median Radius	Shortwave Absorption
CLM-A	CAM-A	CLM	—	Top Layer
CLM-B	CAM-B	SNICAR	200 μm	Top Layer
CLM-C	CAM-C	SNICAR	200 μm	All Layers
CLM-D	CAM-D	SNICAR	100–1000 μm	All Layers

experiments predict surface albedo and vertically-resolved heating with SNICAR, then artificially move all snowpack absorption into the top snow layer. The C experiments predict snow reflectance and absorption as in B, and allow solar absorption to occur realistically in sub-surface layers. Mean optically-effective snow grain sizes range from 50–1100 μm [e.g., *Painter et al.*, 2003]. Experiments B and C predict snow radiative properties using a globally uniform snow radius r_n = 200 μm. This is consistent with sizes determined from field observations of slightly-aged, non-melting snow in Greenland [*Stroeve and Nolin*, 2002] and Japan [*Aoki et al.*, 2000]. The D experiments preserve the snow aging characteristics of CLM with a simple snow age model, increasing r_n based on snow column temperature and time since last snowfall.

[7] We compare model results to three observational snow depth data sets. First, the US Air Force Environmental Technical Applications Center (USAF/ETAC) assembled the only global snow depth climatology that is based on *in situ* measurements covering an annual cycle [*Foster and Davy*, 1988]. The second data set is snow depth derived from the Nimbus-7 Scanning Multi-channel Microwave Radiometer (SMMR) from Nov. 1978 to Aug. 1987 [*Chang*, 1995]. The third data set is based on Advanced Microwave Scanning Radiometer (AMSR-E) global snow water equivalent for 2003 [*Chang and Rango*, 2004]. We converted AMSR-E snow water equivalent to snow depth using the mean TP snow density predicted by CLM (259 kg m^{-3}). Lastly, we compare coupled model air temperature results with the Willmott and Matsuura (WM) [*Willmott and Matsuura*, 2000] and Climate Research Unit (CRU) [*New et al.*, 1999] global observational data sets, and with NCEP re-analysis data [*Kalnay et al.*, 1996].

3. Results and Discussion

[8] Off-line and coupled experiments in Table 1 were integrated for 10 and 15 yr, respectively. In Experiment D the rate of change in global annual mean snow depth is less than 1% yr^{-1} after six years and the net top-of-atmosphere radiative flux is +0.76 Wm^{-2} with no significant trend. All experiments were performed at T42 spatial resolution, approximately 2.8° × 2.8° near the equator. The defined TP region includes about 25 gridcells.

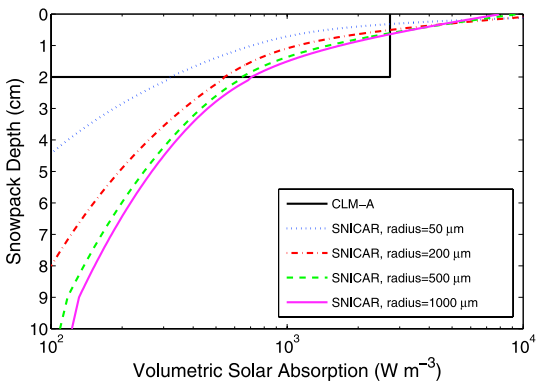

Figure 1. Solar absorption profiles prescribed by CLM and predicted by SNICAR.

3.1. Model Sensitivity to Sub-Surface Snow Heating

[9] SNICAR predicts a significantly more gradual solar radiative absorption profile in snow than CLM prescribes. Figure 1 compares the absorption profiles for a 10 cm snow column assuming TP climate-mean surface insolation of 135 and 137 W m^{-2} in the visible and NIR bands, respectively. SNICAR linearly stratifies snow density based on CLM predictions that density increases from 190 to 590 kg m^{-3} from the surface to 1 m depth. The fractional solar absorption that occurs below 2 cm (the top-layer thickness) with 50, 200, 500, and 1000 μm radius snowpacks is 19%, 36%, 44%, and 47%, respectively. *Brandt and Warren* [1993] suggest about 44% of total solar absorption in an Antarctic snowpack occurs in the top 1 mm. SNICAR estimates about 38% of absorption in a

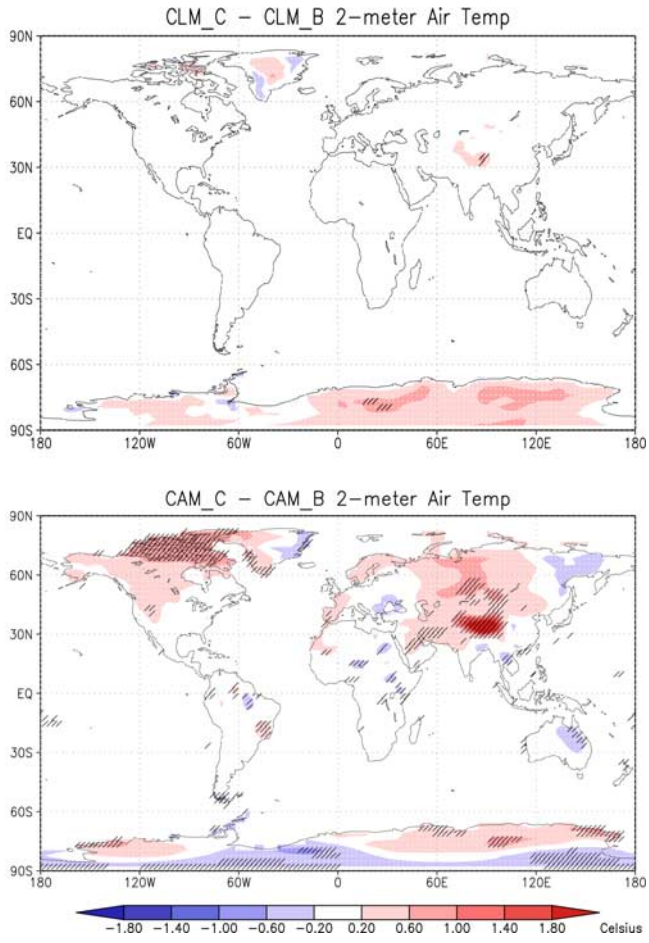

Figure 2. Climatological annual mean difference in 2 m air temperature caused by sub-surface snowpack solar absorption (top) in an off-line land model and (bottom) in a coupled land-atmosphere model. Hatching shows regions where differences are statistically significant at the 1% confidence level.

Table 2. Global Land and Tibetan Plateau (TP) Change in Snow Depth, 2 m Air Temperature, and Surface Albedo Caused by Vertically-Resolved Snowpack Solar Absorption in an Off-Line Land Surface Model and in a Coupled Land-Atmosphere Model

	Snow Depth [m]		Air Temp [°C]		Sfc. Albedo	
	Global	TP	Global	TP	Global	TP
CLM: C−B	−0.05	−0.01	+0.03	+0.23	−0.002	−0.007
CAM: C−B	−0.05	−0.25	+0.10	+2.00	−0.005	−0.138

1 m snowpack occurs in the top 1 mm. Wavelengths longer than about 1 μm are absorbed very close to the surface. Shorter wavelength radiation represents a small but significant fraction of the total absorbed radiation, and penetrates much deeper. Solar radiation penetrates deeper into larger-grained snowpacks. Experiment D accounts for snow grain growth.

[10] Comparison of Experiments B and C isolates the climate effects of sub-surface snowpack heating. Figure 2 shows the mean change (C−B) in 2 m air temperature (T_{2m}) for the off-line and coupled experiments. Table 2 summarizes changes in global land and TP snow depth, T_{2m}, and surface albedo for these experiments.

[11] The heating-induced 5 cm global-mean reduction in snow depth is mostly due to reduced snow accumulation over Greenland and Antarctica, which are perennially snow-covered. Aside from the ice sheets, snow depth changes most over the TP, where snow thickness decreases by 25 cm in the coupled experiment. Local snowfall changed by less than 1%, implying that the snow thickness change is due entirely to increased snow melt and, to a lesser extent, sublimation. We attribute the increased snowmelt to intense wintertime insolation (owing to Tibet's relatively low latitude) and subsequent sub-surface heating. The vertically distributed snowpack radiative absorption predicted by SNICAR and downward thermal diffusion in the C experiments cools the surface snow layer and warms all sub-surface snow layers relative to the B experiments, inducing sub-surface melting. Snow melt triggers atmospheric feedbacks (described below) that enhance snow melt.

[12] The global mean T_{2m} warming in both experiments is small. In the coupled experiment, however, snowpack heating warms the TP by +2.0°C, a highly significant regional change. Moreover, the TP is the only region where statistically significant warming occurs in the off-line experiment.

[13] Table 2 shows that internal snowpack heating reduces surface albedo over the TP by 0.14 and 0.01 in the coupled and off-line experiments, respectively. The striking difference occurs because the coupled experiment allows the ice-albedo feedback mechanism to amplify snowpack-induced climate change over the TP. Snow melt reduces snow depth and therefore snow fraction. Reduced snow fractions expose darker surfaces which absorb more sunlight and, in the coupled experiments, warm the surface air. The ice-albedo feedback loop completes as warmer surface air melts more snow. Mean maximum daily T_{2m} over the TP exceeds the melting temperature (0°) from Apr−Nov with sub-surface heating, but only exceeds 0° from May−Oct without sub-surface heating. Since bulk snow column albedo is identical in these experiments, the surface albedo reduction in Table 2 is due entirely to reduced snow cover and snow depth.

3.2. Model Comparison With Observation

[14] Figure 3 shows seasonal snow depth from the three observational data sets, the original snow model experiments (CLM-A and CAM-A), and our most realistic experiments (CLM-D and CAM-D). While more realistic, the D experiments still neglect potentially significant effects such as absorbing aerosols and vertically-resolved snow grain size.

[15] Both microwave-derived data sets report greater snow depth during winter months than USAF/ETAC, which has less than 2 cm all year. Microwave retrievals overestimate snow mass on the TP by roughly a factor of two because the thin surface atmosphere requires a unique retrieval algorithm which has not been applied, and because seasonally frozen ground produces a snow-like microwave signature (R. Armstrong, personal communication, 2004).

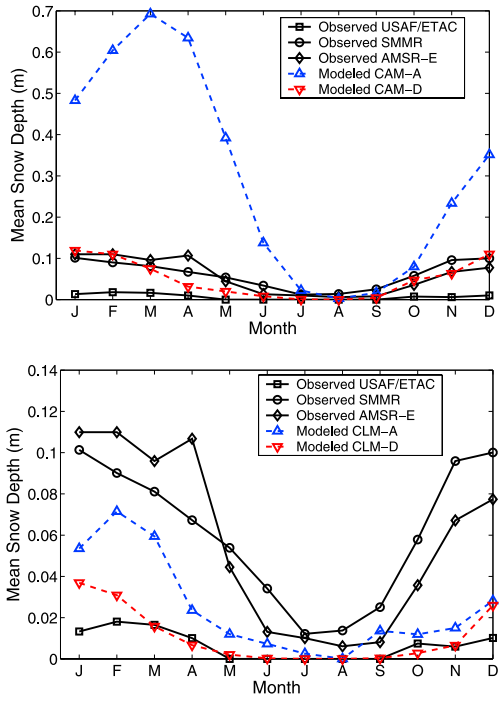

Figure 3. Annual cycle of observed and simulated snow depth over the Tibetan Plateau. (top) Off-line, land-only experiments. (bottom) Coupled experiments.

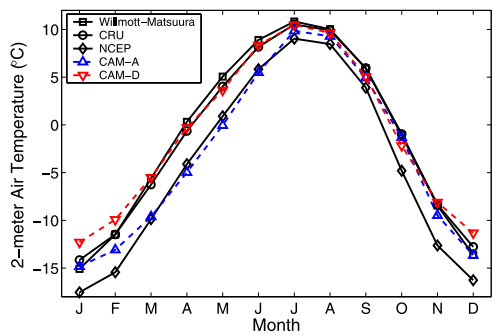

Figure 4. Annual cycle of observed and simulated 2 m air temperature over the Tibetan Plateau.

Furthermore, large errors persist with detection over mountainous terrain and shallow snow [*Chang and Rango*, 2004]. USAF/ETAC may slightly underestimate snow depth because all ground measurements in the TP were made in low valleys.

[16] The off-line experiments are forced with realistic winter precipitation and they predict mean TP Dec–Apr snow depths of 2.3 and 4.7 cm with and without internal snowpack radiative heating (CLM-D and CLM-A, respectively). Likewise, the coupled experiments (CAM-D and CAM-A) predict 8.9 and 55 cm, respectively. The off-line model changes in snow depth are within the margin of uncertainty of our observational data. CAM-A significantly over-predicts winter precipitation on the TP relative to observations [*Willmott and Matsuura*, 2000]. Internal heating and atmospheric warming greatly reduce snow mass, but a slight high bias persists due to excessive snowfall. Further comparison of the coupled experiments with USAF/ETAC data shows that regional snow depth prediction elsewhere is slightly improved or no worse using SNICAR with snow aging relative to the A experiments. In particular, snowpack radiative heating slightly improves simulated annual mean snow depth over the Western U.S. and Eastern Siberia.

[17] Finally, Figure 4 shows the seasonal cycle of T_{2m} over the TP from observations and from Experiments CAM-A and CAM-D. WM and CRU data are climatologies based on station data and interpolations which account for elevation changes, averaged over 1950–1996 and 1961–1990, respectively. The interpolation technique is important due to the sparseness of TP observations. NCEP assimilates model and observational data and, due to sparse T_{2m} TP observations, is probably strongly influenced by the model [*Kalnay et al.*, 1996], which may have snow biases similar to CAM-A. Global mean T_{2m} is 0.14° warmer with vertically-resolved snowpack heating and snow aging relative to CAM-A, and is 2.1° warmer over the TP. CAM-D agrees well with WM and CRU data. NCEP data are colder and closer to CAM-A than CAM-D from Mar–Jul. The largest discrepancies occur in spring, when CAM-A grossly over-predicts snow depth. We expect the more realistic snow depth predicted by CAM-D to improve T_{2m} prediction. However, CAM-D appears to over-predict T_{2m} from Dec–Feb.

4. Conclusions

[18] We used a hierarchy of radiative transfer, off-line land surface, and coupled land-atmosphere climate models to investigate the sensitivity of Tibetan Plateau (TP) climate to sub-surface absorption of solar radiation in snowpacks. Vertically resolving solar heating in snowpacks does not necessarily alter snowpack reflectance, and shows that 20–45% of solar absorption by snow occurs beneath 2 cm. This sub-surface heating significantly alters snowpack evolution and atmospheric warming amplifies snowpack changes via the ice-albedo feedback mechanism. Representing vertically-resolved snowpack heating significantly improves predicted snow depth and 2 m air temperature over the Tibetan Plateau in one coupled land-atmosphere model. It will be interesting to see if other climate models behave similarly.

[19] More physically-realistic snow models such as SNICAR could improve understanding of phenomena related to TP snow cover, such as the South Asian Monsoon and the timing and intensity of spring surface run-off. More work is needed to understand the evolution of snow grain size with time and temperature, the relationship between snow depth and snow fraction, and the effect of absorbing aerosols on snow reflectance and heating. The strong sensitivity of TP climate to internal snowpack heating suggests that dark aerosols may play important roles in snowpack hydrology.

[20] **Acknowledgments.** We thank R. Armstrong, R. Dickinson, K. Oleson, T. Painter, M. Vertenstein, S. Warren, Z.-Liang Yang and two anonymous reviewers for their help and insightful comments. Satellite snow data were obtained from the National Snow and Ice Data Center (http://nsidc.org).

References

Aoki, T., T. Aoki, M. Fukabori, A. Hachikubo, Y. Tachibana, and F. Nishio (2000), Effects of snow physical parameters on spectral albedo and bidirectional reflectance of snow surface, *J. Geophys. Res.*, *105*(D8), 10,219–10,236.

Blanford, H. F. (1884), On the connection of the Himalaya snowfall with dry winds and seasons of drought in India, *Proc. R. Soc. London*, *37*, 3–22.

Brandt, R. E., and S. G. Warren (1993), Solar-heating rates and temperature profiles in Antarctic snow and ice, *J. Glaciol.*, *39*(131), 99–110.

Chang, A. (1995), Nimbus-7 SMMR global monthly snow cover and snow depth, http://www.nsidc.org/data/nsidc-0024.html, Natl. Snow and Ice Data Cent., Boulder, Colo.

Chang, A., and A. Rango (2004), AMSR-E/Aqua monthly L3 global snow water equivalent EASE-Grids V001, http://www.nsidc.org/data/ae_mosno.html, Natl. Snow and Ice Data Cent., Boulder, Colo.

Collins, W. D., P. J. Rasch, B. A. Boville, J. J. Hack, J. R. McCaa, D. L. Williamson, J. T. Kiehl, and B. Briegleb (2004), Description of the NCAR Community Atmosphere Model (CAM 3.0), *Tech. Rep. NCAR TN–464+STR*, Natl. Cent. for Atmos. Res., Boulder, Colo.

Fasullo, J. (2004), A stratified diagnosis of the Indian monsoon–Eurasian snow cover relationship, *J. Clim.*, *17*, 1110–1122.

Foster, D. J., Jr., and R. D. Davy (1988), Global snow depth climatology, *Tech. Rep. USAFETAC TN–88006*, Air U.S. Force, Scott Air Force Base, Ill.

Foster, J., et al. (1996), Snow cover and snow mass intercomparisons of general circulation models and remotely sensed datasets, *J. Clim.*, *9*, 409–426.

Grenfell, T. C. (1991), A radiative transfer model for sea ice with vertical structure variations, *J. Geophys. Res.*, *96*(C9), 16,991–17,001.

Jordan, R. (1991), A one-dimensional temperature model for a snow cover: Technical documentation for SNTHERM 89, *Tech. Rep. Spec. Rep. 91-16*, U.S. Army Cold Reg. Res. and Eng. Lab., Hanover, N. H.

Kalnay, E., et al. (1996), The NCEP/NCAR 40-year reanalysis project, *Bull. Am. Meteorol. Soc.*, *77*, 437–471.

Kurosaki, Y., and M. Mikami (2004), Effect of snow cover on threshold wind velocity of dust outbreaks, *Geophys. Res. Lett.*, *31*, L03106, doi:10.1029/2003GL018632.

Molotch, N. P., T. H. Painter, R. C. Bales, and J. Dozier (2004), Incorporating remotely-sensed snow albedo into a spatially-distributed snowmelt model, *Geophys. Res. Lett.*, *31*, L03501, doi:10.1029/2003GL019063.

New, M., M. Hulme, and P. Jones (1999), Representing twentieth-century space-time climate variability. Part I: Development of a 1961–90 mean monthly terrestrial climatology, *J. Clim.*, *12*, 829–856.

Oleson, K. W., et al. (2004), Technical description of the Community Land Model (CLM), *Tech. Rep. NCAR TN–461+STR*, Natl. Cent. for Atmos. Res., Boulder, Colo.

Painter, T. H., J. Dozier, D. A. Roberts, R. E. Davis, and R. O. Greene (2003), Retrieval of subpixel snow-covered area and grain size from imaging spectrometer data, *Remote Sens. Environ.*, *85*, 64–77.

Schwerdtfeger, P., and G. Weller (1977), Radiative heat transfer processes in snow and ice, in *Meteorological Studies at Plateau Station, Antarctica*, *Antarct. Res. Ser.*, vol. 25, edited by J. A. Businger, pp. 35–39, AGU, Washington, D. C.

Stroeve, J. C., and A. W. Nolin (2002), New methods to infer snow albedo from the MISR instrument with applications to the Greenland Ice Sheet, *IEEE Trans. Geosci. Remote Sens.*, *40*(7), 1616–1625.

Toon, O. B., C. P. McKay, T. P. Ackerman, and K. Santhanam (1989), Rapid calculation of radiative heating rates and photodissociation rates in inhomogeneous multiple scattering atmospheres, *J. Geophys. Res.*, *94*(D13), 16,287–16,301.

Warren, S. (1982), Optical properties of snow, *Rev. Geophysics*, *20*(1), 67–89.

Willmott, C. J., and K. Matsuura (2000), Terrestrial air temperature and precipitation: Monthly and annual climatologies, Cent. for Clim. Res., Dep. of Geogr., Univ. of Del., Newark. (Available at http://climate.geog.udel.edu/~climate)

Wiscombe, W. J., and S. G. Warren (1980), A model for the spectral albedo of snow. I: Pure snow, *J. Atmos. Sci.*, *37*, 2712–2733.

Wu, T.-W., and Z.-A. Qian (2003), The relation between the Tibetan winter snow and the Asian summer monsoon and rainfall: An observational investigation, *J. Clim.*, *16*, 2038–2051.

M. G. Flanner and C. S. Zender, Department of Earth System Science, University of California, Irvine, CA 92697-3100, USA. (mflanner@uci.edu)